AGOR A SUPERCONDUCTING CYCLOTRON FOR LIGHT AND HEAVY IONS*

S.Galès for the Agor project group
IPN Orsay, BP n°1, 91406 Orsay cedex, France and
KVI Gröningen, Zernikelaan 25, 9747 AA Gröningen, Netherlands

Abstract

The main design characteristics of the AGOR K600 superconducting cyclotron are presented with special emphasis on the original aspects of the proposed accelerator : the acceleration of both ligth (protons up to 200 MeV) and heavy ions, the design of the axial injection and central region geometry, the magnet, the RF structures, the extraction system, and the solutions adopted for the cryostat and the superconducting coils. Examples of calculations on the beam dynamics and beam properties will be given. The actual project status is reviewed.

1. Introduction

Following the proposal by the Orsay group[1,2,3] of a variable energy, multiparticle superconducting cyclotron accelerating protons as well as heavy ion beams, a collaboration between French and Dutch national research funding agencies has resulted in the project to study and build such an accelerator to be called AGOR (Accelerator Groningen ORsay). The project will be carried out by two laboratories : l'Institut de Physique Nucléaire d'Orsay (IPN Orsay) and the Kernfysisch Versneller Instituut of Groningen (KVI Groningen).

In December 1985 a contract was signed by the two funding agencies, establishing the operating details of this joint venture. Since that moment the construction of the AGOR machine is underway.

Most of the group activity in 1986 has been devoted to the elaboration of the design of the machine, using the original design proposal as a basis. By now most major parameters are frozen . Procurement of major components (magnet steel, superconducting coils, RF resonators) will be initiated during the course of 1987 and models as well as prototypes will be built. The project is estimated to take 5 to 6 years. The first beams will be produced while the machine is mounted at Orsay before its final installation at Groningen. For construction of the machine 28.1 MHfl is available (approximatively 10 M$). This amount does not include salaries and building costs and is based on July 1985 prices. It is the purpose of this paper to present the main features of the accelerator and its present status. Since details on the cryogenics part and on axial injection will be presented elsewhere[4,5], the emphasis will be more on a broad overview of the machine and discussions of the various choices which have been made.

2. Main Design Characteristics

The machine is a compact, three sector, three dee cyclotron with an effective K=600 and a K_F=220. The feasability of accelerating protons up to 200 MeV implies different requirements for position and geometry of the superconducting coils, for the flutter poles and magnet structures as well as for the RF operating range as compared to other superconducting cyclotrons[6]. Fig.1 shows the major components, the split-cryostat containing the two paires of superconducting coils, the yoke walls, the geometry of poles and valleys, the RF structures and the axial injection line.

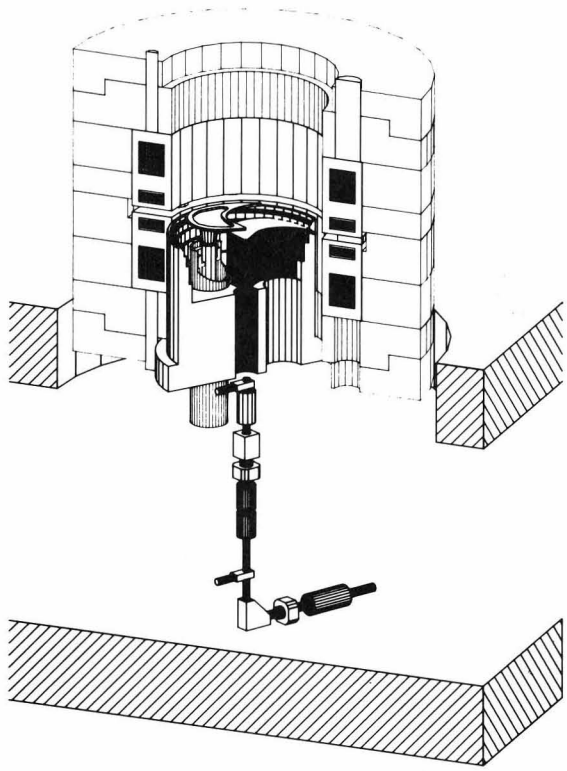

Fig.1- Simplified cutaway view of the magnet assembly.

The cyclotron will have T/A versus Z/A operating curves as shown in fig.2, using external ion sources (duoplasmatron for light ions : (p,d,^{3}He) and ECR source for heavy ions with a charge to mass ratio ranging from 0.5 to 0.1).

An operating range of 24 to 62 MHz for the accelerating frequency using the three harmonics modes (h = 2,3 and 4) has been chosen. The regions of the operation for the 2nd, 3rd and 4th harmonics are shown in fig.2. The majority of beams energy (10 to 72 MeV/nucleon) will be accelerated on the 3rd harmonic, the more relativistics ions will use the 2nd harmonic due to limitations of the maximum RF frequency to 62 MHz and of the maximum allowable vertical components of the electric field E_z in the inflector ($E_z \leq 25$ kV/cm) For the low energy part of the diagram (10-6 MeV/nucleon) the harmonic mode h = 4 will be used, the choice being to limit the minimum frequency to 24 MHz in order to minimize the mechanical displacement of the short-circuit and therefore the length of the RF resonators. The design of a central geometry compatible with the 3 harmonic modes has been considered to be a basic feature of the design and has been successfully achieved in the study[4]. The change from one harmonic mode to the others implies only a change of the inflector.

The operating diagram (Bo, Z/A) plane, where Bo is

the central field value is given in fig. 3. The bending (K) and focusing (K_F) limits are shown, together with lines of constant energy per nucleon. A wide operating range

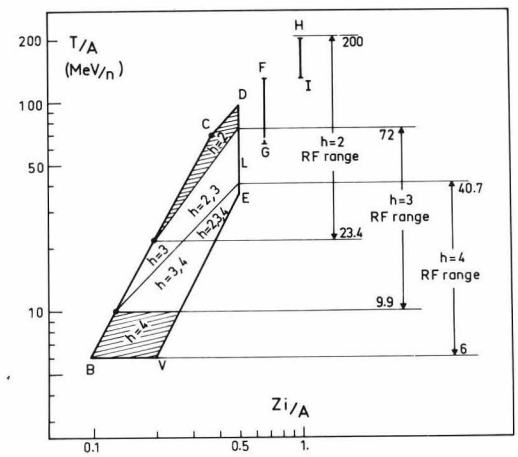

Fig.2 - Ions energy vers Z/A in MeV/per nucleon and boundaries of the operating range of the RF frequency (24 to 62 MHz) using the three harmonics modes h = 2,3,4.

in terms of magnetic field ($1.75 \leq B_o \leq 4.05$ Teslas) has been achieved, assuming that desaturation effects will be small and taking into account the limits imposed by the $\nu_R + 2\nu_Z = 3$ resonances. This allows a variation of more than a factor of two in energy for the $^3He^{++}$ and Z/A = 0.5 ions.

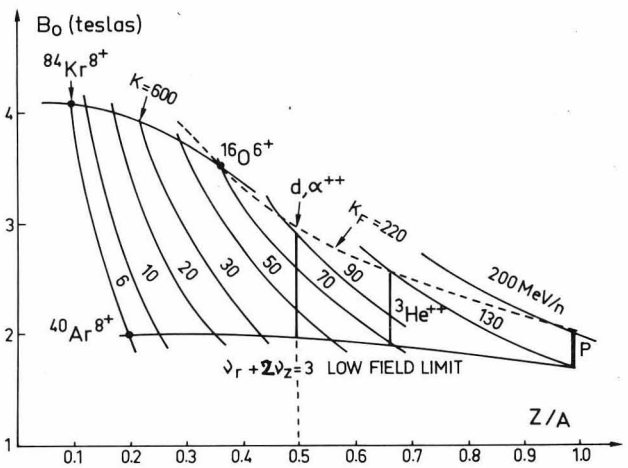

Fig.3 - Operating diagram in the (B_o,Z/A) plane. bending K, focusing K_F and low field limits are indicated. Constant energy per nucleon lines are also displayed.

A fundamental problem in the acceleration of protons to an energy of approximately 200 MeV is the rapid increase of ν_R with energy up to the forbidden $\nu_R = 1.5$ resonance. In our machine this problem has been avoided by reducing the scalloping of the orbits. This has been achieved by introducing an additional valley along the axis of each hill sectors. The appropriate shapes of the average magnetic field were achieved using the following guidelines :

(i) search for the position and geometry of a first pair of superconducting coils producing the radial gradient necessary for the acceleration of the more relativistic particles (protons, $^3He^{++}$, Z/A = 0.5). This property is obtained using a flat coil close to the median plane,

(ii) determination of the characteristics of a second coil able to compensate for this gradient and producing an average field independent of the radius,

(iii) among the various possibilities for the average contribution of the iron of the poles, we have chosen a design leading to a constant contribution as a function of the radius.

These choices lead to the magnet geometry shown in figs 4 and 5.

The major machine parameters are listed in table I.

Table I - Cyclotron parameters

Bending limit	K = 600
Focusing limit	K_F = 220
Pole diameter	= 188 cm
No of sectors	= 3
	No spiral for R< 30 cm
Spiral coefficient	1/20 rd/cm at R = 70 cm
	1/40 rd/cm at R = 88 cm
Min hill gap	= 7 cm
Max valley gap	= 84 cm
Main coil 1 current density	= 4271 A/cm² max.
Main coil 2 current density	= 3270 A/cm² max.
Central field main-max	= 17.5 - 40.5 K gauss
No of trim coils	= 15
Max current in trim coils	= 500 A
Number of Dees	= 3 in valleys
RF Range	= 24 to 62 MHz
Operating harmonics	= 2, 3, 4
Peak dee voltage at R = 0	= 85 kV

3. Magnet Structure

A vertical cross-section of the accelerator is presented in fig.4 while a median plane sketch is displayed in fig.5. The magnet will have a cylindrical iron yoke consisting of 8 cast steel rings, and two removable cylindrical poles.

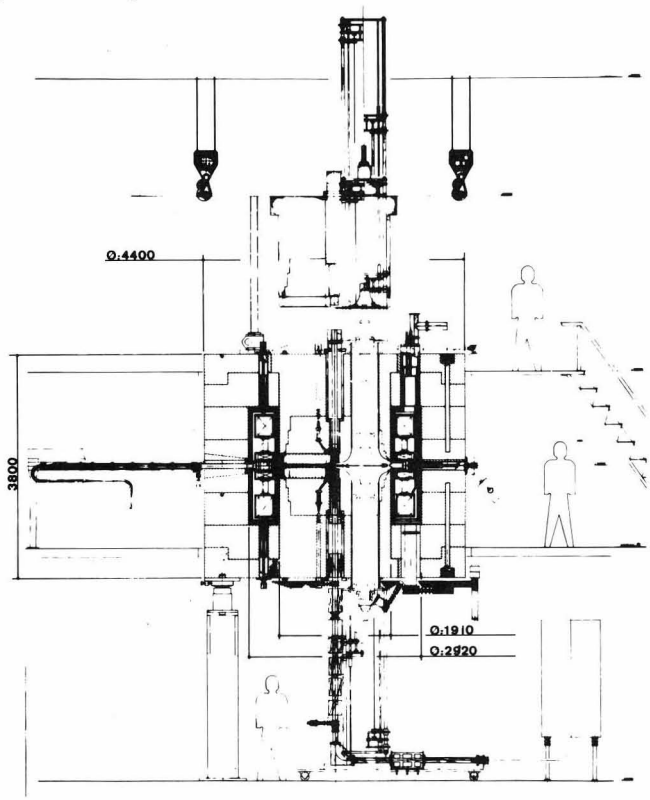

Fig.4 - Vertical cross-section of the cyclotron. All dimensions are in cm.

Each of these poles serves as a mounting base for three spiralled iron flutter poles.

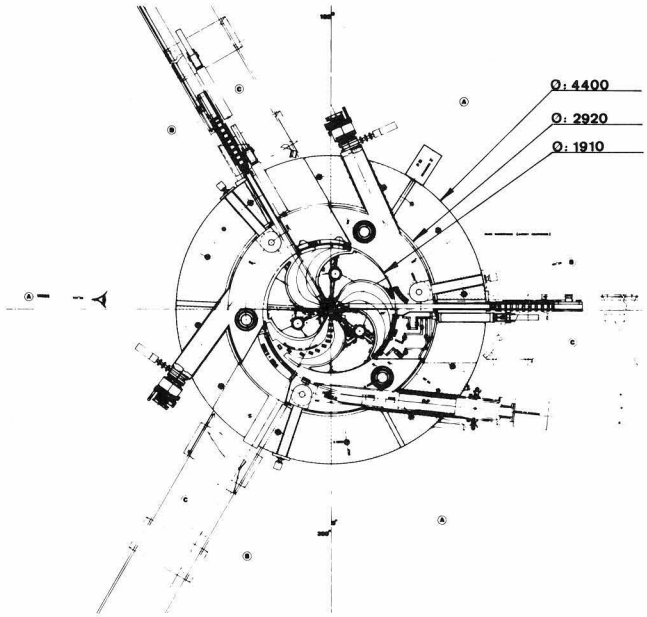

Fig.5 - Median plane sketch of the cyclotron. All dimensions are in cm.

The main magnet parameters are given in table II.

Table II - Magnet parameters

Pole radius	= 94 cm
Yoke inner radius	= 146 cm
Yoke outer radius	= 220 cm
Yoke full heigth	= 380 cm
Lifting range of the upper pole	: 2.50 m
Steel = cast, carbon content	≦ 0.04%
Total weight	= 350 T.

The open space between the poles and yoke which accomodates the cryostat and the superconducting coils has a radial width of 52 cm and a total axial heigth of 200 cm. A novel feature of the design is the study of a split-cryostat[5] which provides excellent access to the mid plane.

Since the attractive force between the poles at full excitation is around 1400 tons, deformations of the yoke are anticipated. These effects have been calculated, neglecting in a first step the various holes, using analytical formulaes. The results show that the yoke should have a axial deformation of less than 0.2 mm, by large within elastic limits. More detailed calculations using three dimensional computer code CASTEM are underway.

The angular width of the hill sectors increases from 36° at their initial radius of 7 cm to a width of 55° at R = 40 cm and stays constant up to R = 70 cm. From then on the sectors widths decrease, reaching 48° at R=88 cm. In this region the Archimede spiral coefficient lays from 1.8 ra/m to 4.26 ra/m . From R = 88 cm to R = 93 cm the sectors are radial, in order to decrease axial focusing ν_z , in the region where $\nu_R + 2\nu_z = 3$ resonance limits the machine performance.
As mentioned above, additional small valleys are introduced in the middle of the flutter poles (see fig.5). Their width is roughly 1/3 of the hill width and then depth is approximately 21 cm.

Fig.6 shows the hill and valley profiles. As can be seen from the figure the hills are split into two parts in order to provide space for winding the fifteen trim coils around the upper part. The valley profile has an approximately semi-elliptic radial cross section which has been ajusted to produce the desired shape of the iron contribution to the average field.

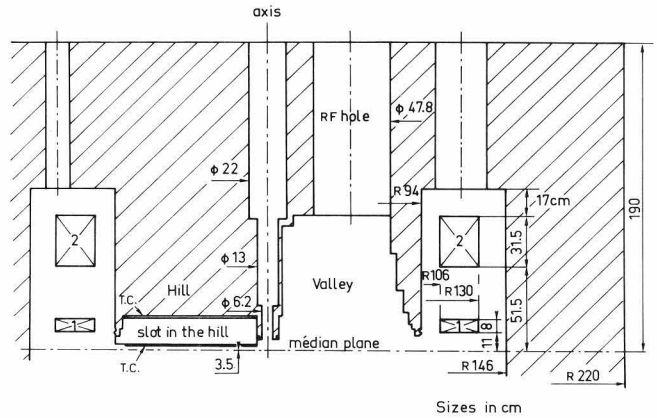

Fig. 6 - Hill and valley radial profiles. All dimensions are in cm.

The axial hole provided for axial injection purpose has a diameter of 12.4 cm in the part closest to the median plane, increasing to a diameter of 25 cm to give more room for devices such as buncher, diagnostics, steering plates, solenoïds, etc...

The fifteen trim coils will be similar to those already developped at MSU and Milano[7]. Each coil has 1 layer of 5 turns of 6 x 6 mm² conductor and will carry a maximum current of 500 A. The trim coils will be covered by a vacuum enclosure, which separates them from the machine vacuum. This enclosure will at the same time be the RF liner.

4. The superconducting coils and the split-cryostat

As pointed out before the superconducting coils system consists of a pair of outer coils generating the desired overall field profile and a pair of inner coils close to the mid plane that generate a radial field gradient depending on the ion to be accelerated. The current density needed in the two pair of coils, J_1, J_2 in order to produce an isochronous field for all ions and energies have been computed. The corresponding operating diagram in shown in fig.7 where constant B_o and Z/A lines are also plotted. The diagram shows that J_1 and J_2 are always positive, a situation which simplify the analyses of the forces and stresses on the coils. The geometry of the coil system is unique in the sense that a large gap exists between the inner and the outer coil of 0.325 m. Due to this design the axial Lorentz force between the coils are greatly reduced (6.6 MN) in comparison with other coils systems for superconducting cyclotrons (17.0 MN) allowing for only six rods support a 4.2 K between the coils in the mid-plane. As a consequence it was possible to design a split-cryostat in which room-temperature access is provided to most of the middle plane enabling an easy install (and withdrawell) of extraction elements and diagnostics probes. An overall view of the cryostat and coils is given in fig.8. The total weigth of the cryostat + superconducting coil system is of about 30 tons.

In table III are listed the main characteristics of the superconducting coils.

The superconducting coils will be fully vacuum impregnated to reduce the risk of electrical shorts between the windings and to enhance the mechanical stability.

Thermal stability of the coils is improved by liquid helium in direct contact with the winding package at all sides.

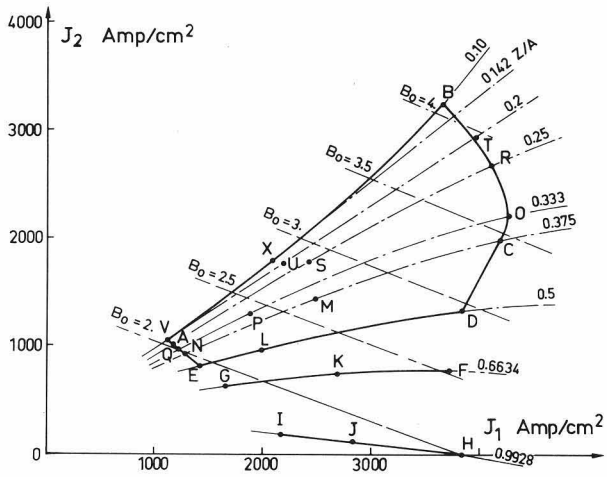

Fig.7 - Cyclotron operating diagram in the (J_1, J_2) plane.

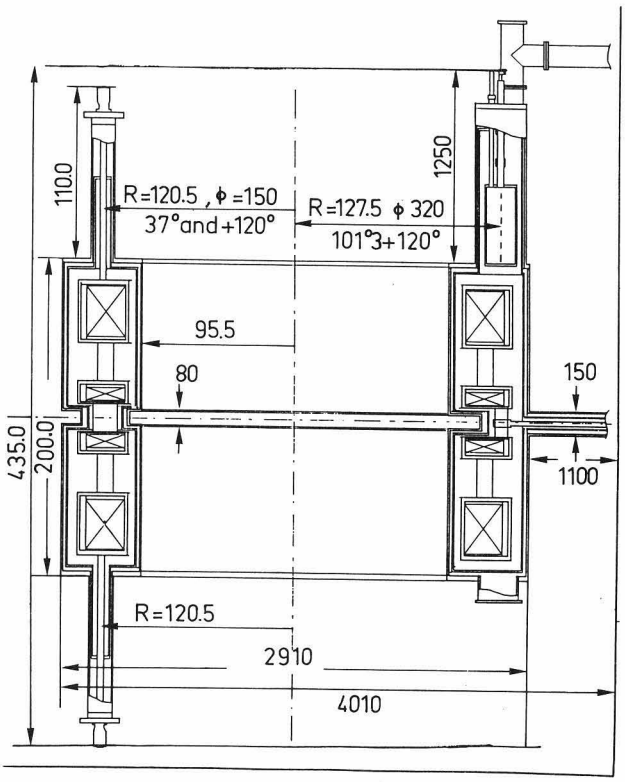

Fig. 8 - Overall view of the cryostat and the coils. All dimensions are in cm.

In the design of the cooling system much effort is given to enhance the overall efficiency. The detail of this design is discussed in a contribution to this conference [5]. The basic features are an liquefier operating effectively as a refrigerator, current leads cooled by a separate refrigeration system and a 80 K radiation shield mounted inside the cryostat vacuum to reduce the heat load on the superconducting coils. It will be cooled by a separate system. No liquid nitrogen will be used either for cooling the 80 K radiation shield, or for precooling.

The total cooling power of the system is 1300 W at 80 K simultaneously with 60 W at 20 K.

Table III - Characteristics of the superconducting coils

	Coil 1	Coil 2
Inner radius	1.06 m	1.06 m
Outer radius	1.30 m	1.30 m
Width	0.08 m	0.315 m
Max overall current density	42.71 MA/m²	32.65 MA/m²
Max field strength	3.64 T	4.74 T
Conductor cross section (bare)	3.03x5.31mm²	5.5x8.6 mm²
(insulated)	3.53x5.71mm²	6.0x9.0 mm²
Cu : Sc ratio	19	26
Superconductor	NbTi, rutherford cable copper substrate	
Nominal transport current	861 A	1763 A
Critical current (3.64T, 4.6K)	1435 A	2963 A
Critical temperature	7.5 K	6.5 K
Conductor length (per coil)	7.1 Km	11.4 Km
Conductor mass (per coil)	1200 Kg	5700 Kg

5. Magnetic field properties and beam dynamics

The field produced by the magnet structure discussed before is excellent. The average field has been calculated using the code TRIM with stacking factors to simulate hills, shims and poles, a model similar to that employed at MSU[7], over a grid of 21 values in the J_1 J_2 plane which covers the operating range.

The average field produced by the iron is plotted in fig. 19 at 4 different excitations including the lowest and the highest ones. The results of the calculations matches to a good accuracy our expectation for the iron contribution to the average field. With the main coils and iron contribution isochronism can be obtained for all ions with modest trim coils currents. A diagram of the power dissipation in the trim coils for various working points of the accelerator is given in fig. 10.

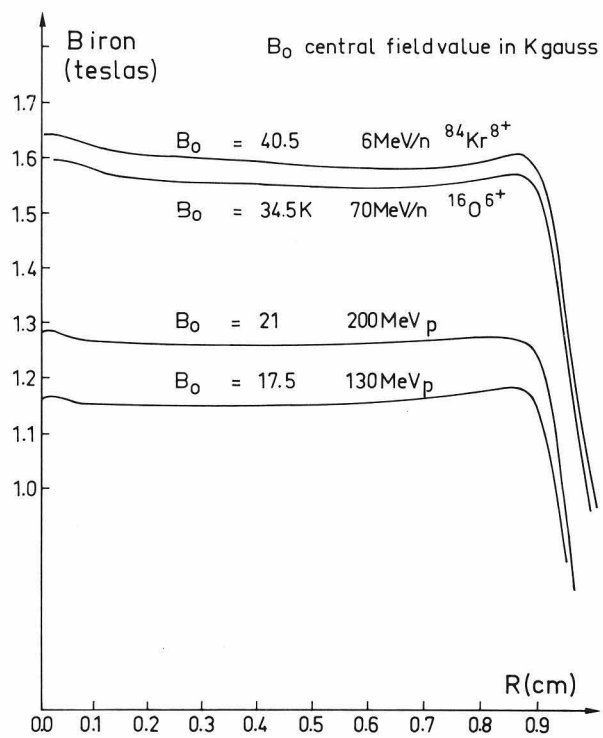

Fig.9 - Contribution to the average magnetic field produced by the iron at four different main coils excitations.

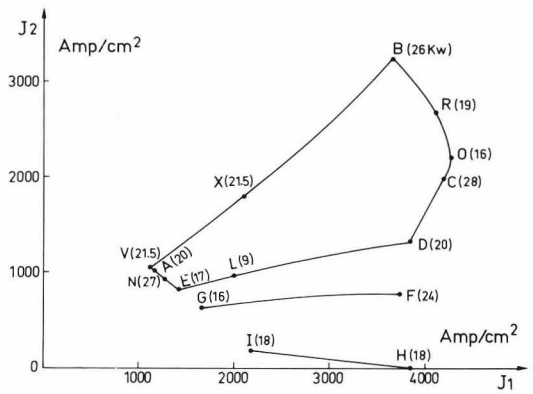

Fig. 10 - Power dissipation in the trim coils for various points of the operating diagram.

The flutter, as calculated by the uniform saturation approximation, provides adequate focusing. As an example, fig. 1 presents the working path in the (ν_R,ν_z) plane for 200 MeV protons and 9.6 MeV/n $^{84}Kr^{21+}$ ions.

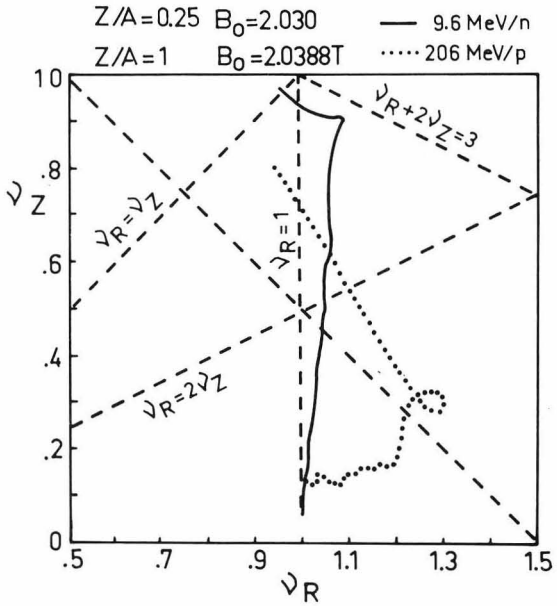

Fig. 11 - Working path (ν_R,ν_z) for 200 MeV protons (and 9.6 MeV/n $^{84}Kr^{21+}$ ions.

A multiparticle version (up to 100 particles)[8] of the SPIRAL GAP code has been used to study the beam dynamics prior to extraction.

The proximity of resonances once identified are investigated using the code TRACY[9] at a given energy. The transfer of beam emittance from the center (R≅10cm) to the extraction has been studied for a serie of representative points of the operating diagram. Initial conditions are defined by a phase acceptance, an initial value of the injected beam emittance and the assumption than the beam is matched to the optics of the cyclotron at r = 10 cm. The characteristics of the beam at the entrance of the first extraction element is given below for the case of 200 MeV proton beams.

Ion	Phase acceptance	Initial emittance (mm-mrd)	Energie Extraction (MeV)	Radius (m)	ε_x,ε_z (mm-mrd)	$\Delta E/E$ (10^{-3})
p	± 15°	18	204.65	.890	4.9,.23	12
	± 3°	18	204.95	.893	.5,.22	0.5

6. Extraction

As seen in fig.5, the extraction is accomplished by an electrostatic deflector(ESD), 38° long and two electromagnetic channels (EMC1, EMC2) positionned in two consecutive hills. A third electromagnetic channel EMC3 followed by two quadrupoles Q_1,Q_2 located inside the yoke are used to confine the beam along the extraction path. The main parameters of the extraction system elements are listed in table IV.

Table IV - Main parameters of the extraction system elements

Element	θ_{IN}	θ_{OUT}	E (kV/cm)	ΔB (KG)	$\partial B/\partial_x$ (Kgauss/cm)
ESD	48°	86°	85	-	-
EMC1	168°	208°	-	3	-
EMC2	290°	330°		3	.35
EMC3	350°	20°		1.5	
Q1					1.5
Q2					- 1.5

Note the rather moderate electrical field necessary in the electrostatic deflector .Due to the large range of magnetic fields and therefore the variation of the optics axis of each beam, the electrostatic deflector must be radially movable by about 1.4 cm. In addition its shape must change sligthly in order to fit all extraction trajectories. The deflector will consist of two parts, which can rotate around each other. A sketch of a prototype is shown in fig. 12. The septum will consist for its first part of 0.05 mm thick Mo strips in order to enhance the transmission efficiency.The beam properties through the extraction elements are illustrated in fig.13 for two characteristics ions (200 MeV/protons and 9.6 MeV/n $^{40}Ar^{10+}$).

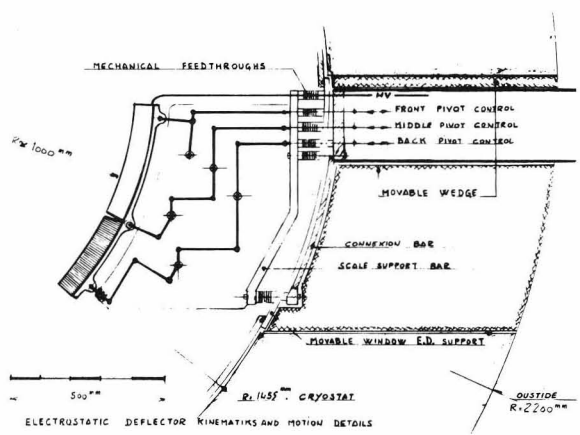

Fig.12 - Sketch of a prototype for the electrostatic deflector.

7. Axial injection and central region geometry

The axial injection system for the superconducting cyclotron is designed to operate with 3 ion sources : a light ion source able to deliver up to a few 100 μA beams of H and He^{++} an E.C.R. for heavy ions and polarized light ion source. The injection line, compatible for the operation at Orsay and at KVI is shown in fig.15. It consists of unit transfer matrix cells and of 2 matching sections (one for the different ion sources, the other for the cyclotron). Because of the polarized ions, the transport line before the 90° electrostatic spherical deflector is based on electrical quadrupoles. A buncher operating at the RF of the cyclotron and common to the 3 harmonic modes h = 2,3,4 will be placed about 50 cm

from the median plane to take into account various limiting parameters (source noise, axial field etc...).

The central region geometry has been designed in conjunction with a spiral inflector. A design study taking into account the space availability, voltage limitation, R.F. shielding, as well as large gain in the first 2 electrical gaps has been carried out. The electrical equipotential surfaces have been measured on a 5 to 1 scale model allowing a detailed study of the horizontal and vertical motion.

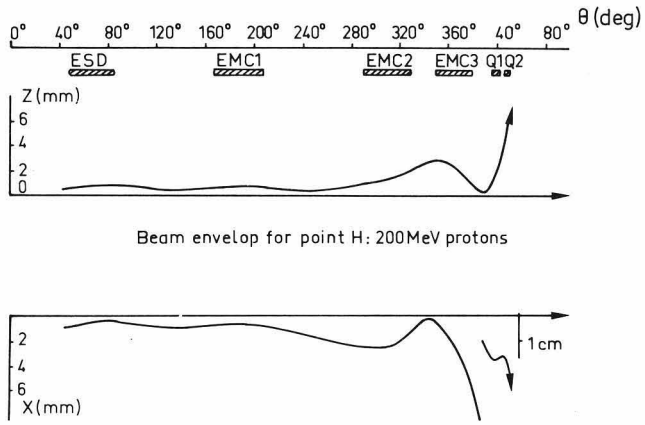

Fig. 13 - Radial and axial envelopes of a 200 MeV protons and 9.6 MeV/n $^{40}Ar^{10+}$ extracted beams.

Phase and geometrical vertical focusing can be achieved using a magnetic bump on one hand and posts and steps on the other hand. A central region geometry representation and the three trajectories h = 2,3 and 4 are shown in fig. 16.

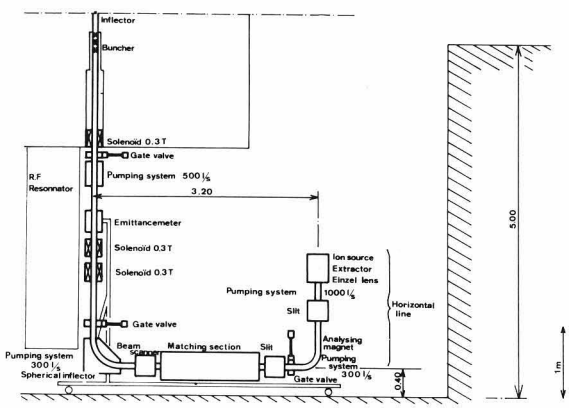

Fig.14 - Schematic lay-out of the axial injection line.

First results show that one obtains a vertical acceptance compatible with an E.C.R. emittance (75 mm-mrd) and an off-centering between 1 and 3 mm in the first five turns. Introduction of magnetic corrections is in progress to improve the characteristics.

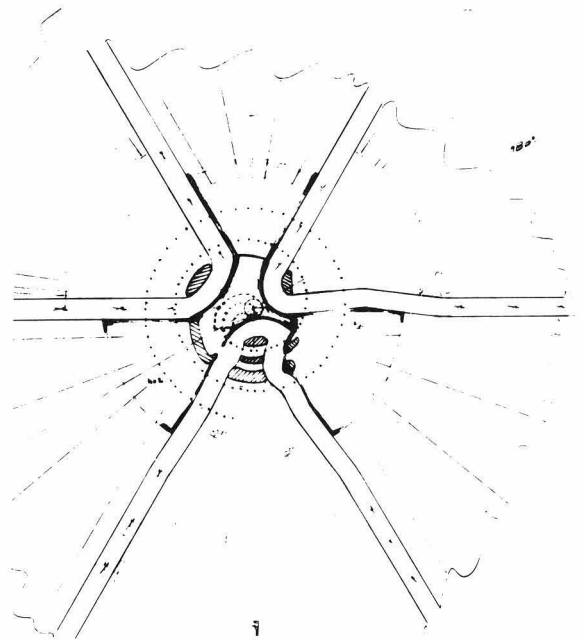

Fig.15 - Central region geometry design and trajectories for h = 2, 3 and 4.

8 - R.F System

The R.F system consist of three compact half-wave length resonators with continuous and smooth connection to the Dees.

Using the specified injection R.F voltage vs frequencies fig.(16) and the last mechanical drawings a new computation of the resonator has been made[11]. We have carefully adjusted the shape and position of the stem

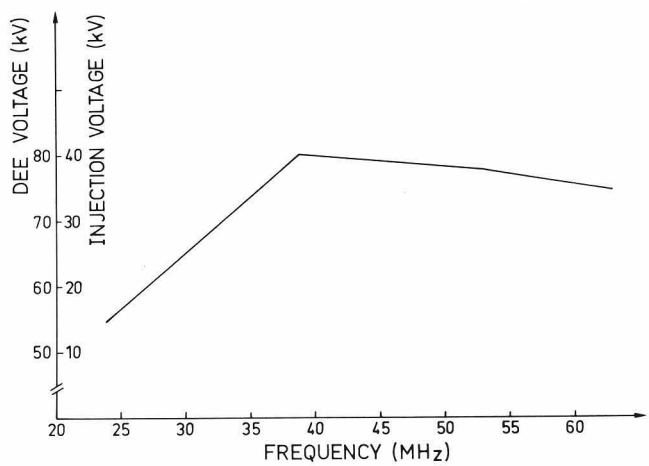

Fig. 16 - Injection RF voltage (peak) vs frequencies.

to electrode connection in order to obtain a moderate radial increase of the voltage without a too high current density in the short-circuit, minimizing at the same time the R.F power and the length of the stem. It is seen from the curves in fig. 17 that the maximum power at 62 MHz is limited to 38 kW with a current density around 40 A/cm in the short-circuit. The short-circuit movement does not exceed 1.65 meter from 24 to 62 MHz.

Experiments[12] with a specially built resonator have shown that the sliding contacts, which we have developped, withstand current densities over 80 A/cm at 27 MHz,

in good agreement with calculations. From these measurements and from calculations it is estimated that at 62 MHz current densities up to 55 A/cm can be accepted. This gives a sufficient safety factor. Experiments at 62 MHz are under way and will be finished at the end of this year.

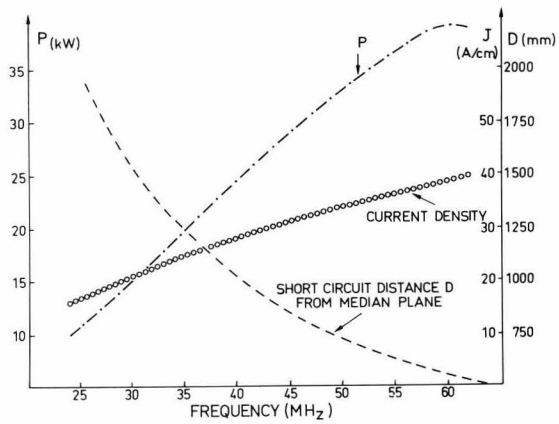

Fig. 17 - Power, current density, short circuit position vs frequencies.

The complete pre-mechanical studies are finished and a full-scale model resonator will be built to determine precisely the resonant frequencies and the voltage and current distribution and also to test the fine tuning and the coupling systems.

Furthermore the design and construction of various components of the R.F regulation system, such as stable and accurate discriminators phase shifters etc ... has been started.

Project status

Presently studies on the installation of the machine at Orsay are underway. A general lay-out of the building installation is shown in fig. 18.

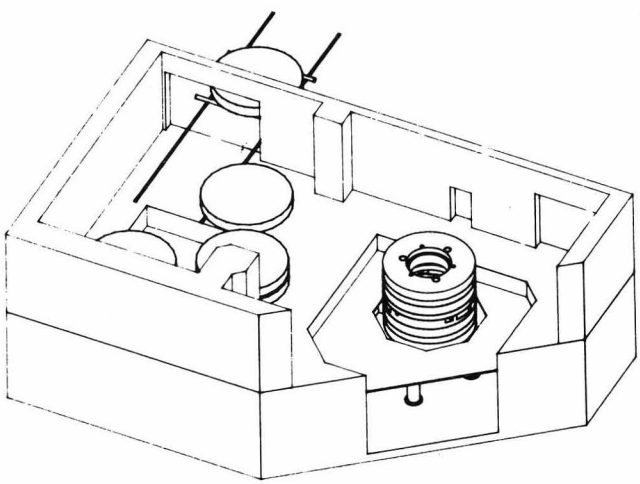

Fig. 18 - Plan view of the installation of the machine in the old ALICE building at Orsay.

The cyclotron will be located in the building where the ALICE accelerator system was installed. The definition of an appropriate crane, the modification of the building walls and the construction of the cyclotron pit are expected to begin in the first month of 1987.

Experimental tests on the various elements of the injection line will be undertaken on a standard test bench and on a similar axial injection line of the MEDICYC cyclotron[10]. Bid for tenders for the magnetic yoke and iron of the sections will be placed at the end of this year.

A half-scale model of the R.F cavity will be designed and constructed while detailed mechanical and thermodynamics studies will be pursued.

A prototype of the electrostatic deflector is being built.

For the cryogenic system, experiments are conducted at Delpht University on the current leads and on the radiation shield.

Elements of the control system which has a modular architecture consisting of a number of mirocomputers are already being tested.

It is anticipated that the main components of the cyclotron (magnet steel, R.F resonators and amplifiers, superconducting coils and cryostat will be ordered during the course of next year.

* Work jointly supported by the INSTITUT NATIONAL DE PHYSIQUE NUCLEAIRE ET DE PHYSIQUE DES PARTICULES(IN2P3), France and by the foundation STICHTING VOOR FUNDAMENTEEL ONDERZOEK DER MATERIE (FOM), Netherlands.

References

1 . I.P.N. Orsay project - First machine design studies A. Laisné, 9th Int. Conf. on Cyclotron and their applications, Caen (Sept. 81) 203.

2 . Le projet de cyclotron à bobines supraconductrices et l'ensemble accélérateur associé, rapport final sur les études théoriques et techniques de faisabilité, Report IPNO-GEPL Orsay (juin 83).

3 . Minimum spiraling solutions upgrading the capacility in light ion acceleration of a superconducting isochronous cyclotron.
A. Laisné, 10th Int. Conf. on cyclotron and their applications, East Lansing (Mai 84) 288.

4 . J.P. Schapira, Axial injection system for the superconducting cyclotron AGOR. Contribution to this conference.

5 . K. Pieterman, Design study of the AGOR superconducting coils and criogenic system, Contribution to this conference.

6 . Application of superconductivity in cyclotron construction.
H.G. Blosser, 9th Int. Conf. on Cyclotron and their applications, Caen (Sept. 81) 147 and references herein.

7 . G. Bellomo, D.A. Johnson, P. Miller and F.G. Resmini Nucl. Ins. and Methods, 180 (1981) 285.

8 . D. Potaux, A multiparticle version of the SPIRAL GAP Code (unpublished).

9 . D. Potaux and J.M. de Coster, TRACY a ray-tracing code (unpublished)

10. P. Mandrillon et al., A 60 MeV proton cyclotron associated with a new target design for neutrontherapy ; 10th Int. Conf. on Cyclotron and their applications, E. Lansing, 1984, p.475.

11. C. Bieth, Parametres fondamentaux des resonateurs principaux d'AGOR, Internal report NT/HF/30/04/86

12 J. Lébris, C.Guillaume, Resultats des essais de contact, type AGOR 1 à 27 MHz, NT/HF/24/01/86.